DOI: 10.13009/EUCASS2017-260

Experimental analysis of heat transfer in cryogenic combustion chambers on Mascotte test bench

Julien Pichillou*, Philippe Grenard**, Lucien Vingert**, Gillian Leplat***, Philippe Reulet***
*CNES, Launcher Directorate
52 rue Jacques Hillairet 75612 PARIS CEDEX 12
**ONERA, The French Aerospace Lab, F-91761 PALAISEAU, France
***ONERA, The French Aerospace Lab, F-31055 TOULOUSE, France

Abstract

Combustion experimental test at subscale is a key element for the knowledge improvement of the design of liquid rocket engine. Within the frame of a CNES ONERA common research program, the MASCOTTE test bench has been used to gather an important experimental database of H2/O2 fire tests. In order to progress in the characterization of the test set up, a campaign was performed dedicated to the determination of the combustion chamber wall temperature dispersions for different gas/gas operating points.
The identification of the heat fluxes on the injector face plate requires an improvement of post processing methods. A new methodology was then developed and validated by ONERA in order to solve the inverse heat conduction problem for complex 3D geometry with embedded local measurements.

1. Introduction

One of the main challenges in liquid rocket engines is the estimation of the heat fluxes released at the combustion chamber wall. The wall heat fluxes are difficult to predict precisely due to complexity of the chemical and fluid dynamic phenomena occurring in the combustion chamber. The simulation tools (CFD or analytic approach) used for wall heat fluxes prediction need then to be compared with experimental results. Unfortunately, the instrumentation of real engine is generally really poor compared to the data needed for assessment of the prediction methods. Combustion experiments on a dedicated subscale test set up can be designed in order to build exhaustive set of data recorded in representative operating conditions.
ONERA and CNES collaborate on a common research project aiming at improving the knowledge of the heat transfer in the combustion chamber. This project combines experimental studies and numerical analyses.
The experimental tests take place on MASCOTTE test bench: an experimental subscale combustor water-cooled and fed with five injection elements operating with LOX/GH2 or GOX/GH2. The objective of the experimental part of this project is to build a thermal database (wall temperature, heat flux) and a visualization database in order compare the values measured during tests with classical correlations. The experimental database is also used to give inputs to build validation cases for the numerical analyses. The numerical part of the project aims at developing methods in order to simulate the combustion chamber with a special focus on interaction between combustion chamber internal flow and chamber walls.
This paper will present the latest hot firing campaigns and the post-processing methods developed for the analysis of the test data.
A firing campaign performed in 2014 aims at improving the characterization of the test setup. The relative location of the temperature sensor with regard to the injector is studied. The objective of this test campaign is to assess the test setup measurement uncertainties.
Test data post-processing method is also very important: in the cylindrical wall, heat flux computation is based on the thermal gradient between two temperature sensors located near the walls (one on the hot gas side and the other on the cooling water side). For the heat flux on the injector head, this method is not applicable as it is not possible to implement pairs of thermocouple to measure the thermal gradient. A new post-processing method based on inverse heat conduction method is then applied in order to assess heat fluxes.

DOI: 10.13009/EUCASS2017-260

2. Hot firing campaigns

1.1 Mascotte test bench

Experimental investigations of wall heat fluxes started in 2010 on the Mascotte cryogenic test facility of ONERA. The bench itself, as well as the water-cooled combustion chamber used for these tests have been described in several papers ([1],[2],[3],[4][5]) and will be briefly describe hereafter. Several versions of the hardware were developed and manufactured for the different points of interest of the project. The first one is the “thermal” version (Fig. 1a) used in the present study; it consists of an injection head with an interchangeable face plate (instrumented non-cooled or non-instrumented non-cooled or non-instrumented water cooled), two cylindrical segments (L = 200 mm, D= 56mm) and an axi-symmetric nozzle.

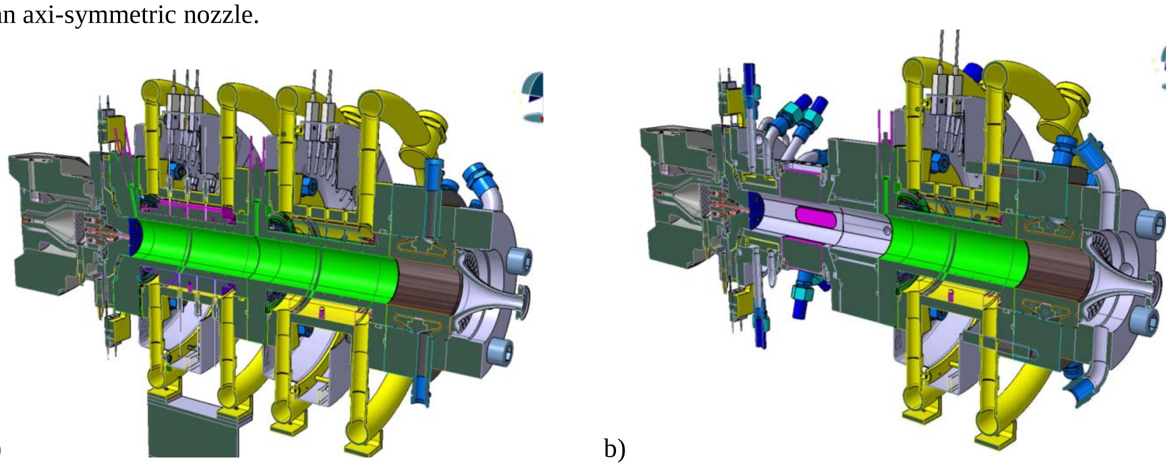

a) b)

Figure 1 – The water-cooled combustion chamber – Thermal version (left) and Visualisation version (right)

In this “thermal version”, the two cylindrical segments are water cooled and instrumented with 17 pairs of thermocouple brazed into the combustion chamber walls: one located on the hot gas side and the other on the cooling water side. Those thermocouples are aligned with three azimuthal locations, monitoring the longitudinal evolution of the temperature. With the assumption that longitudinal and azimuthal temperature gradient are small compared to the radial one, the heat fluxes can be computed from the temperature measurement by solving a 1D heat equation problem.

In the second version (Fig. 1b), devoted to optical diagnostics, the first segment is replaced by a visualization module with four optical ports.

Fluids are injected by means of five identical coaxial injectors, consisting in a central tube delivering LOX, surrounded by an annular GH2 outer jet. In the vertical injection plane, four injectors are placed around a circle, every 90°, and the fifth injector is placed at the center.

The hydrogen is always injected gaseous at a temperature varying from ambient down to 100 K, while the oxygen can be gaseous at room temperature or liquid at approximately 90 K. The operational domain covers a large range of pressures, from subcritical to supercritical (1 to 7 MPa), as well as a large variety of mixture ratios from 1 to 7, allowing investigations of both gas generator and thrust chamber applications. Ignition is performed thanks to a GO2/GH2 torch igniter paced in the first segment.

1.2 Injector Head rotation campaign

CONFORTH test set up acceptance was achieved during several campaigns performed between 2010 and 2014: successive campaigns were executed with various injection conditions (gaseous and liquid oxygen, gaseous hydrogen with reduced temperature). Those campaigns permitted to acquire an important database in terms of heat fluxes, temperature levels and flames visualizations (see [3], [4] & [1]).

Heat fluxes have been deduced from temperature measurements, leading to a database which helps to consolidate the design procedure and also can be used for numerical simulation validation (cf. [5]).

As presented previously, the temperature measurements are organized along 3 generating lines which are located in three different quadrants (figure 2):

- A : on generating line lined up with an external injector
- B : between 2 external injector generating lines
- C : between the positon A and B

DOI: 10.13009/EUCASS2017-260

It is supposed that thanks to the combustion chamber symmetry, the thermal flux map around the circumference can be deducted from the measurements located along theses 3 generating lines.

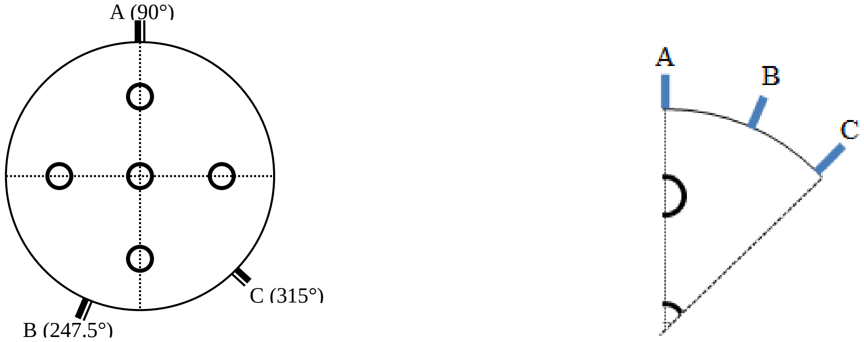

Figure 2: Temperature sensors implementation on cylindrical combustion chamber walls

In order to validate this symmetry assumption, it has been decided to perform a new hot fire campaign. During this campaign, experimental conditions (mixture ratio *r*, pressure *P*) are reproduced several times with different injector-to-thermocouple position. In practical the injector head is rotated by 45° while the cylindrical segments (i.e. the instrumented generating lines) stay at the same position (figure 3). It is then possible to record successive temperature measurement at specific position with different thermocouple pairs. Any measurement error (calibration error, thermocouple defect) should be detected by the comparison of the measurement performed at the same position by another thermocouple.

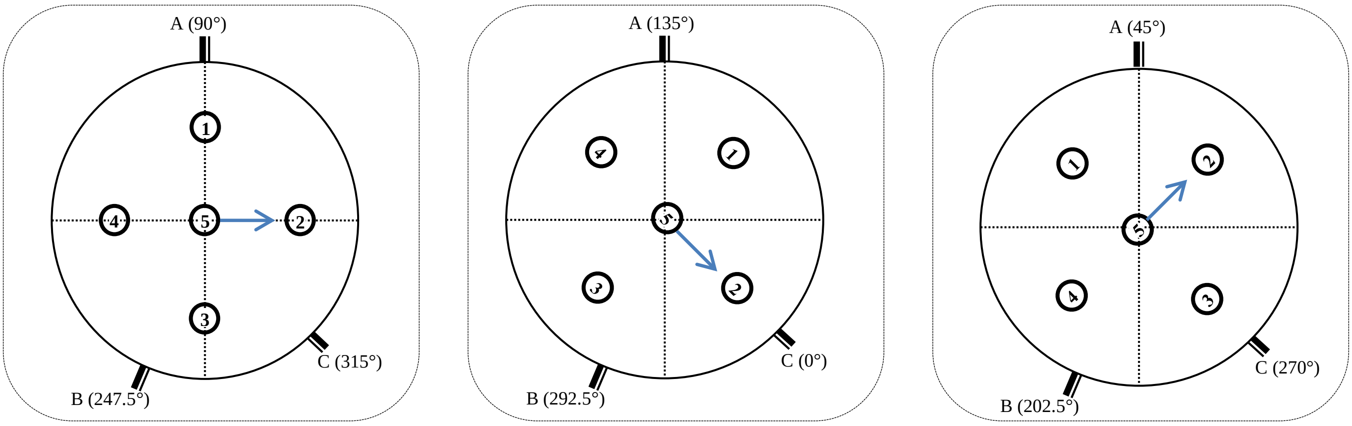

a) Reference position

b) Injector head rotated by +45°

c) Injector head rotated by -45°

Figure 3: Thermocouple to injector head positions

Test bench configuration

The injection face plate used during this campaign is the non-instrumented water cooled injection head. This water cooled face plate enable to perform long duration fire and then to reach steady state not only for the flow inside the combustion chamber but also for the temperatures on the combustion chamber wall. Five shear injectors are fed with gaseous hydrogen gaseous oxygen. One injector is on the central axis of the chamber and the 4 others are equally spaced on a 30mm diameter circle. The combustion chamber is composed of the 2 two instrumented cylindrical segments. The engine is closed by a axisymmetric nozzle cooled with an internal helium film.

Operating conditions

Two different operating points were selected for the gas-gas conditions:

- Operating point #1: low O/F ratio r=2, 40 bar
- Operating point #2: high O/F ratio r=6, 40 bar

For each operating point, the measurements were repeated at least two times for each injection head position. A graph presenting the operating points obtained during the tests is presented on figure 4.

DOI: 10.13009/EUCASS2017-260

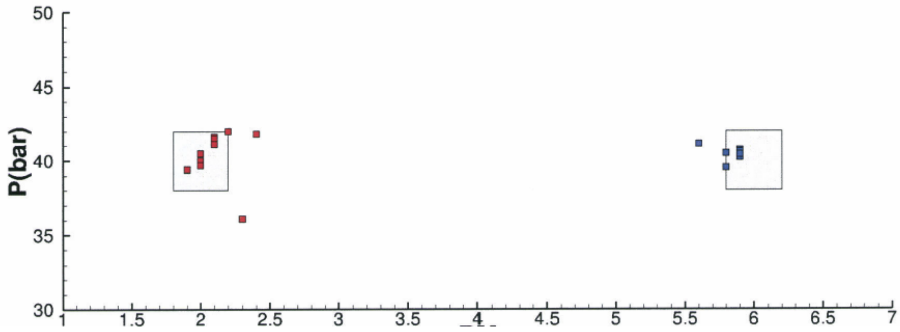

Figure 4: operating points obtained during the tests

Results

The temperatures recorded during the tests are presented in the following paragraph. The temperature measurements are normalized by a reference temperature, T_{ref}. The normalized temperature, defined as $T^* = T/T_{ref}$ is then plotted versus the normalized longitudinal coordinate, $x^* = x/L_c$.

The measurements are gathered accordingly to their position w. r. t. the injectors. The figure 5 represents the temperature profiles for the position 0° (facing injector), 45° (between injectors) and 22.5° (intermediate position).

For the low mixture ratio, the temperatures tend to decrease along the longitudinal axis. In the first part, the temperatures decrease is strong, while in the second half temperatures tend to stay uniform and converge.

In the first section, the temperatures dispersion is striking. The temperatures recorded at the given position can vary by tenth of degrees depending on the thermocouple generating line used to perform the measurement. It is unlikely that this variation for the successive measurement performed at a single position result from operating conditions variation during the test since the flow rates, temperatures were stable and reproducible during the tests.

The dispersion can more probably be linked with the temperature sensors. The temperatures profiles recorded for each generating line are plotted on figure 6. It can be noticed that the temperature dispersions on generating line A and C (whatever their position with regards to the injectors) are smaller than the dispersions observed for the different positions 0° and 45°.

So the temperatures dispersions seem more related to uncertainties linked to the temperatures sensors. The thermocouples were calibrated prior to being brazed in small holes drilled in the combustion chamber walls. Small uncertainties of the radial position of the thermocouples during the brazing procedure can lead to significant temperature scattering.

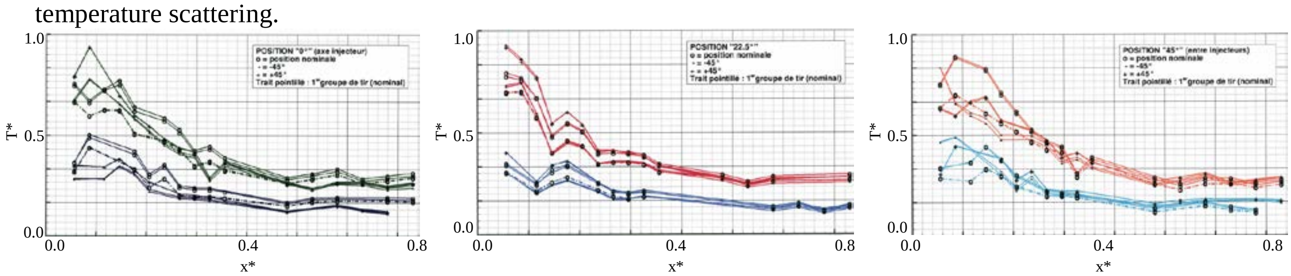

Figure 5: Temperature evolutions for the different positions w. r. t. injectors: 0° (left), 22.5° (middle) and 45° (right) P=40, r=2

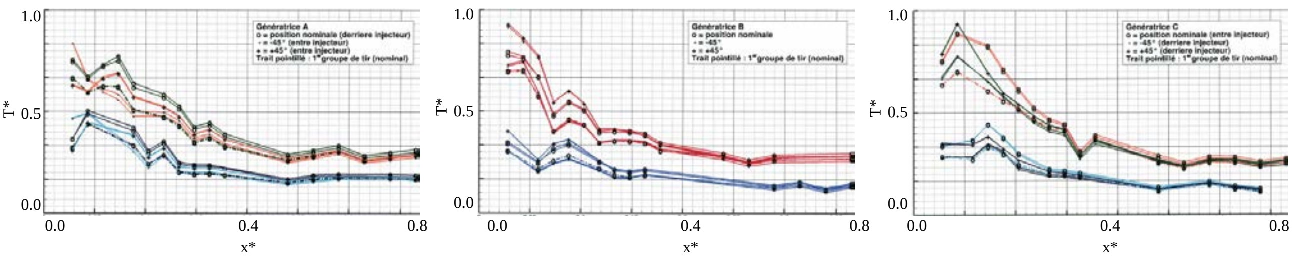

Figure 6: Temperature evolutions for the different generating lines: A (left), B (middle) and C (right) - P=40, r=2

DOI: 10.13009/EUCASS2017-260

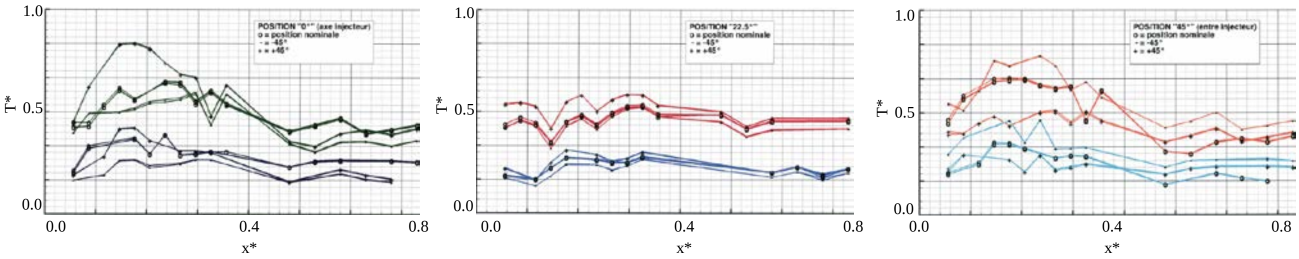

Figure 7: Temperature evolution for the different positions w. r. t. injectors: 0° (left), 22.5° (middle) and 45° (right) P=40,r=6

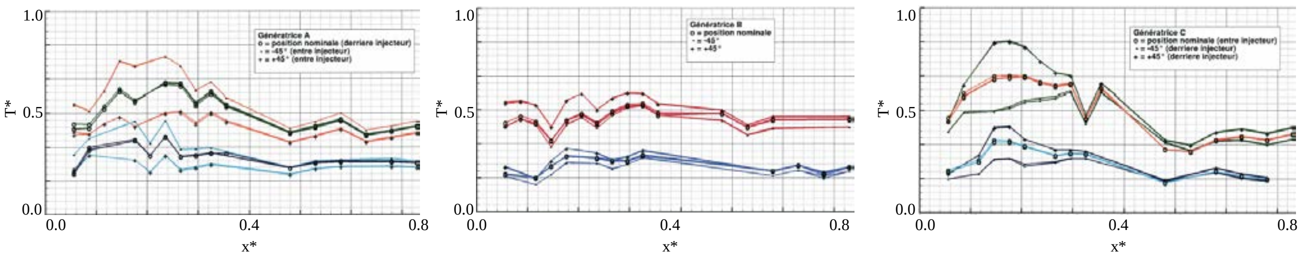

Figure 8: Temperature evolutions for the different generating lines: A (left), B (middle) and C (right) - P=40,r=6

For r=6 (figure 7), the temperatures evolution along longitudinal axis present globally a maximum along the first part of the combustion chamber but the temperature decrease is less evident than for the low mixture ration runs. For 0° and 45° positions, temperature profiles present a bump with maxima around the first quarter of the length. The temperature profiles for the 22.5° do not show any evident trend. The temperature scattering in the first part of the combustion chamber is obvious. Temperatures tend to converge in the second half of the combustion chamber.
As for the low mixture ration runs, the temperature profiles recorded on a specific generating line are plotted on a same chart (figure 8). For these high mixture ratio runs, the temperature dispersions on a generating line tend to be as big as the dispersions obtained for the profile at fixed position w. r. t. injectors.

It is possible to represent the temperature map measured during the different run on a single map. Assuming that the thermocouple measurement can be reported on this map accordingly to their position with regards to the injection head the cartography can be created.

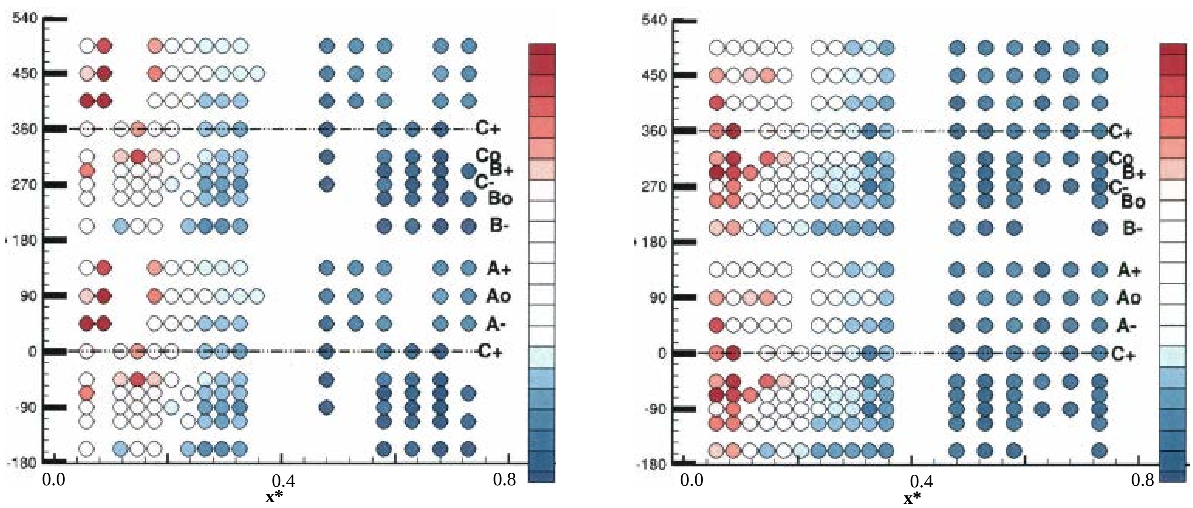

Figure 9: Temperature map: cold side on the left / hot side on the right – (P=40,r=2)

On the representation presented on figure 9 and 10, the temperatures are presented on more than 360° in order to highlight the temperature repartition. The injector’s positions are marked by the black rectangle on the left (0°, 90°, 180° and 270°).
For the low mixture ratio (figure 9), the temperature map do not reveal any specific pattern but it is evident that the temperature repartition on the combustion chamber wall is not symmetric. For the high mixture ratio (figure 10), it is possible to observe a hot region in the quadrant [0°;90°]. The wall temperatures are colder in the opposite quadrant [180°,270°].

DOI: 10.13009/EUCASS2017-260

Those observations lead to the conclusion that the flow inside the combustion chamber can be dissymmetric.

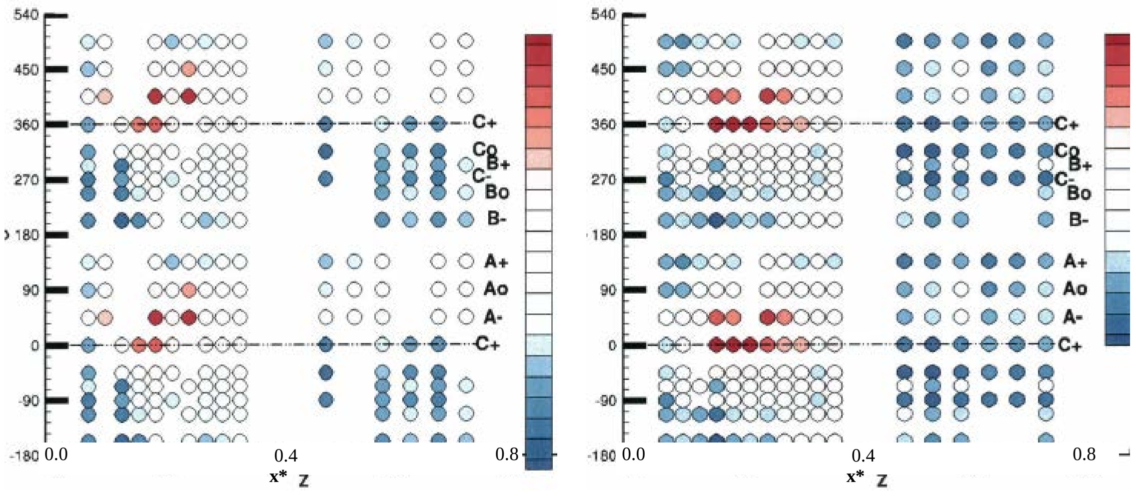

Figure 10: Temperature map: cold side on the left / hot side on the right – (P=40,r=6)

The different analyses of the temperatures obtained during test, provided a large amount of data. Those data can be used to provide validation cases for the numerical simulations. As explained before, temperature dispersion observed during test remains not totally understood. It is then useful to treat the large amount of data in order to define mean temperature profiles for each operating point. The dispersion on the recorded temperatures can be treated as an uncertainty range for the numerical to experimental comparisons. For each operating point, 6 data sets are extracted: 2 for the head injector head in the reference position, 2 for the -45° position and 2 for the +45° position. For each thermocouple location the mean value and the standard deviation are computed. The results are presented on figure 11 and 12.

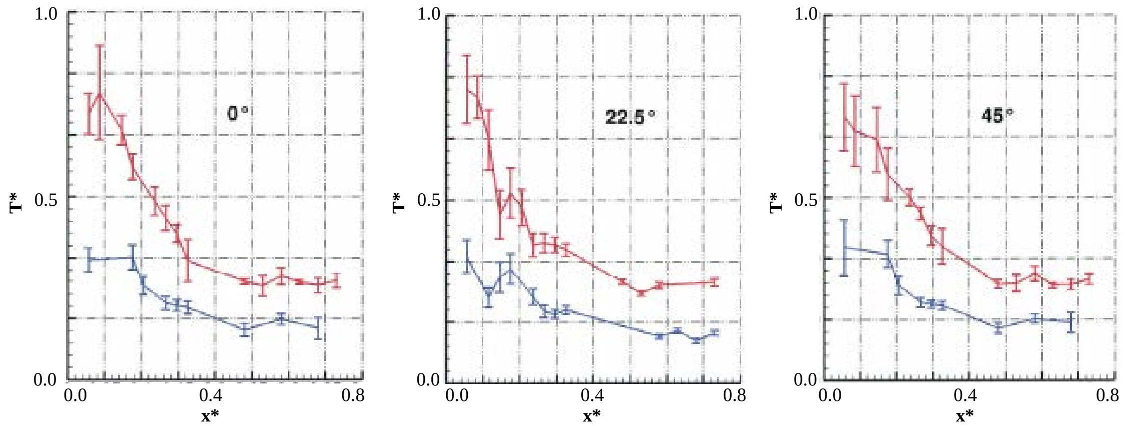

Figure 11: Mean temperature and standard deviation evolutions – P40, r=2

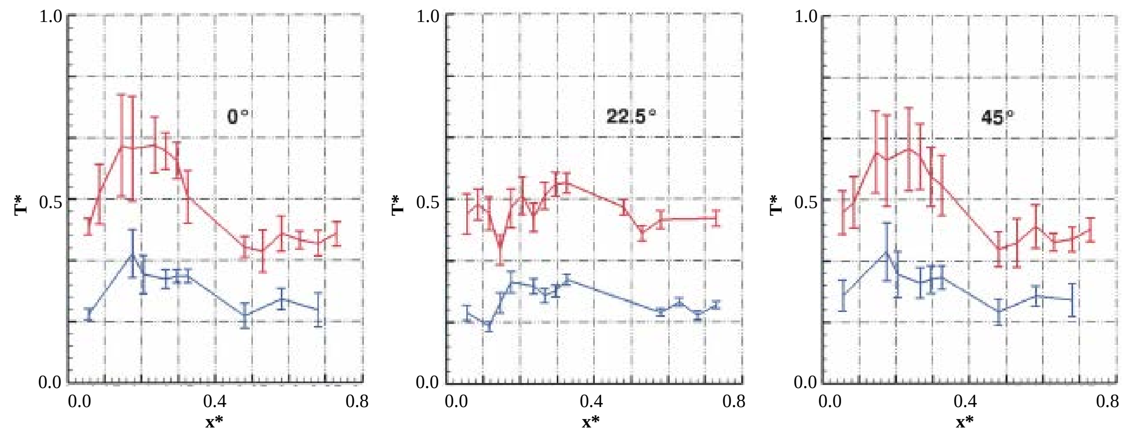

Figure 12: Mean temperature and standard deviation evolutions – P40, r=6

DOI: 10.13009/EUCASS2017-260

2. Test data post processing methods

2.2 Heat fluxes in cylindrical wall

As said before, the two cylindrical segments are instrumented with 17 pairs of thermocouple brazed into the combustion chamber walls: one located on the hot gas side and the other on the cooling water side.
Under the assumption of a purely radial heat flux in cylindrical coordinates, at steady state, the heat flux is solution of the equation:

$$\frac{\partial}{\partial r}\left(r\lambda(T)\frac{\partial T}{\partial r}\right) = 0$$

which is easily integrated in the solution:

$$r\phi(r) = \lambda_m \frac{T_{PG} - T_{PE}}{\ln\left(r_{PE}/r_{PG}\right)}$$

under the assumption of a quasi-linear dependency of the conductivity with respect to the temperature. (λ_m is the value of conductivity $\lambda(T_m)$ at the mean temperature between hot gas side T_{PG} and water cooled side T_{PE}.

2.3 Heat fluxes in injector head

The non-cooled injector head is equipped with 14 thermocouples installed 0.5mm under the surface facing the combustion chamber. The sensor locations are presented on figure 13. The distribution of the sensors over the disc surface is mainly due to implementation constraint: it is necessary to route the wire to the outer diameter of the injector head.

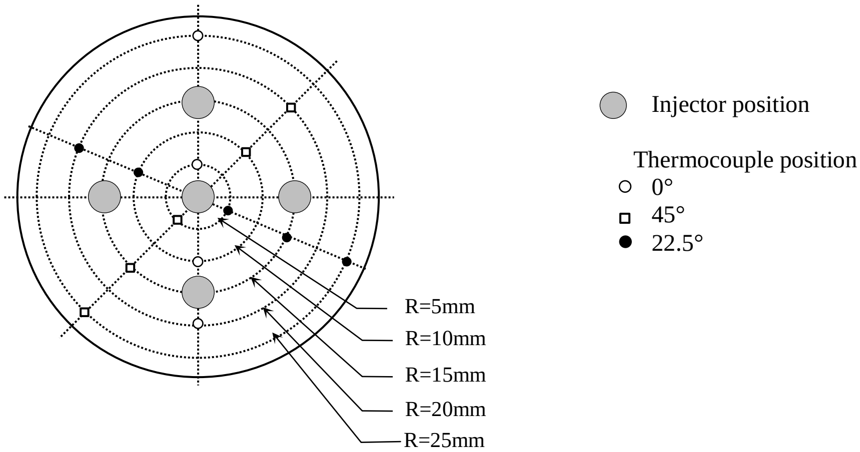

Figure 13: Injector head temperature sensors map

In order to calculate the heat fluxes received by the injector head, a first calculation assuming a semi-infinite heat transfer in the injector head body was performed. To use this method, it is necessary to assume the specimen geometry is close to a 1D problem. For the injector head, this assumption is questionable as the thermocouple locations are close to the injectors. The heat exchanges due to the propellant circulation in the injector generate a complex configuration and the 1D approach is not valid.
Such a complex 3D geometry requires to be treated with an adequate method in order to calculate the heat fluxes applied on a body on the basis of temperature measurements inside or on the backside of the body. This problem is called inverse heat conduction problem. The inverse heat conduction problem is a mathematically ill-posed problem since the solution is sensitive to errors in input data. ONERA developed a method able to solve efficiently the inverse heat conduction problem [6]. The resolution is based on the minimization of a function representing the sum of the differences between the observations (measured temperatures Y_i^{n+j}) and the calculated temperatures T_i^{n+j} at the same position in the least square sense.

$$R = \sum_{i=1}^{N_{arr}} \sum_{j=1}^{r} \left(Y_i^{n+j} - T_i^{n+j}\left(q_1^{n+1}, \dots, q_{N_{av}}^{n+1}, \dots, q_1^{n+r}, \dots, q_{N_{av}}^{n+r}\right)\right)^2$$

DOI: 10.13009/EUCASS2017-260

The Beck sequential algorithm is used to minimize the functional: this method is based on sequential estimation of a time-varying boundary condition and the use of future time steps.

$$R = \sum_{i=1}^{N_{arr}} \sum_{j=1}^{r} \left(Y_i^{n+j} - T_i^{n+j}\left(q_1^{n+1}, \dots, q_{N_{av}}^{n+1}\right) \right)^2$$

The minimization of R conducts to:

$$\forall h, \frac{\partial R}{\partial q_h^{n+1}} = -2 \sum_{i=1}^{N_{arr}} \sum_{j=1}^{r} \frac{\partial T_i^{n+j}}{\partial q_h^{n+1}} \left(Y_i^{n+j} - T_i^{n+j}\left(q_1^{n+1}, \dots, q_{N_{av}}^{n+1}\right) \right) = 0$$

$$\begin{bmatrix} \Delta q_1 \\ \dots \\ \Delta q_{N_{av}} \end{bmatrix} = \begin{bmatrix} S'_{11} & \dots & S'_{1N_{av}} \\ \dots & \dots & \dots \\ S'_{N_{av}1} & \dots & S'_{N_{av}N_{av}} \end{bmatrix}^{-1} \begin{bmatrix} D_1 \\ \dots \\ D_{N_{av}} \end{bmatrix}$$

$$S'_{lh} = \sum_{i=1}^{N_{arr}} \sum_{j=1}^{r} \left(S_{T_i, q_l^{n+1}}^{n+j} S_{T_i, q_h^{n+1}}^{n+j} \right)$$

$$S_{T_i, q_h^{n+1}}^{n+j} = \frac{\partial T_i^{n+j}}{\partial q_h^{n+1}}$$

$$D_l = \sum_{i=1}^{N_{arr}} \sum_{j=1}^{r} \left(Y_i^{n+j} - T_i^{n+j}\left(q_1^{n}, \dots, q_{N_{av}}^{n}\right) \right) S_{T_i, q_l^{n+1}}^{n+j}$$

It is necessary to calculate the sensitivity coefficients S that represent the temperature rise at the thermocouple location per unit surface flux area. This step can be performed thanks to a direct heat conduction computation.

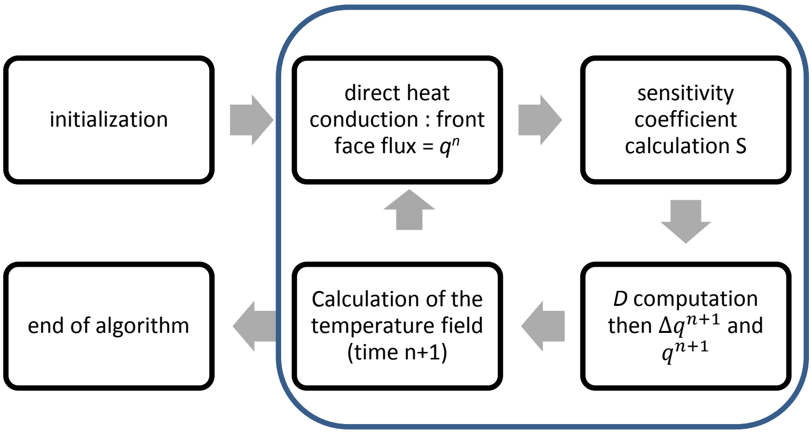

Figure 14: Flux identification algorithm

The method initially in place at ONERA is developed to treat simple parallelepiped geometries with temperature measurements taken on the unexposed surface by infrared thermography. The inverse method is integrated in ONERA's software THIDES which also includes the direct thermal model.

It is necessary to adapt this method to the injector head configuration with local temperature measurements and more complex geometries. The existing method integrated in THIDES must be interfaced with a thermal solver able to treat complex geometries. ACACIA solver, part of CEDRE ONERA CFD Platform for energetics, can be used to solve such direct heat flux problems. Compared to existing method with detailed infrared thermographic measurements), the number of punctual measurement points on CONFORTH injector head is very limited. It is then necessary to introduce additional assumptions on the thermal fluxes distribution.

DOI: 10.13009/EUCASS2017-260

Methodology improvements

In order to validate the adaptation of the existing method to local temperature measurements and a complex geometry, a step by step approach was used:

- Adaptation to complex geometries with surface measurements
- Application to local temperature measurements.

These required numerical developments were conducted in order to interface the inverse heat transfer resolution with ACACIA solver. Dedicated tests performed in the BLADE test facility are used to gradually validate the adaptation.

Test bench description

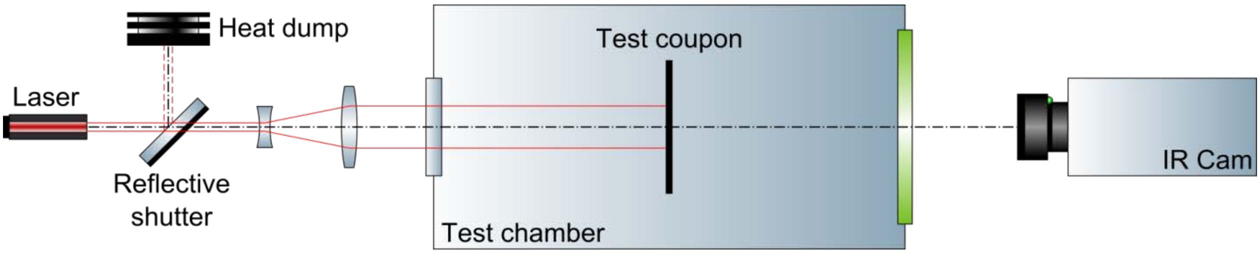

Figure 15: Blade test set up

The BLADE test facility (figure 15) consists of a test coupon (metallic plate) enclosed within a test chamber equipped with optical accesses. An infrared laser beam is used to heat the test coupon on one side. The temperature is measured on the opposite side using infrared thermography or thermocouples. The laser beam has a Gaussian distribution and it is calibrated so that it is possible to know precisely the incoming heat flux on the front side. The fluxes calculated thanks to the inverse heat method can then be compared to the fluxes generated by the laser.

The pressure and the temperature of the test chamber are regulated in order to have a good control of the operating conditions. In particular, the tests are performed at low pressure in order to avoid heat transfer by convection. A coolant fluid circulates in a copper coil fitted onto the chamber wall in order to control the test chamber temperature.

Test configurations

Several tests configurations are tested successively in order to validate the methodology improvements:

- C1 : Square (80x80x3mm) plain specimen with infrared thermography to obtain back face temperatures
- C2 : Cylindrical plain specimen (Ø80, 5 mm thick) with infrared thermography to obtain back face temperatures
- C3: Cylindrical specimen (Ø80, 5 mm thick) with 4 holes (Ø10mm) at injectors' locations. Cork caps are inserted in the holes in order to impose adiabatic boundary conditions. The temperatures of the back face were still measured by infrared thermography.
- C4: Cylindrical specimen with cooling tube at injectors' locations. The temperatures of the back face were measured thanks to 12 thermocouples. The temperatures sensors are distributed (figure 16 right) on 3 radial positions (r=5mm, 10mm, 20mm and 30mm) so that they are lined up along 3 generating lines considering the sample symmetry (45°, 22.5° and 0°).

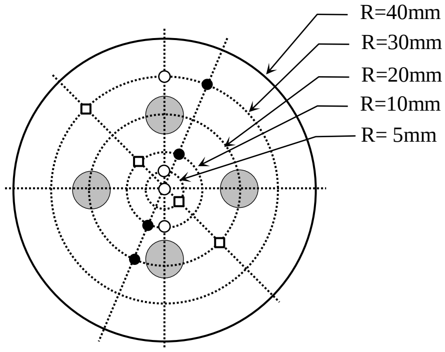

Figure 16: Test samples (left) and temperature sensor positions for configuration C4 (right)

DOI: 10.13009/EUCASS2017-260

BLADE test procedure

Prior to testing, the test sample is inserted within the test chamber. The test chamber wall temperatures are controlled by the fluid circulation. The test chamber is pumped down to 5 mbar.

Temperature recording starts at t=0s. At t=1s, the reflective shutter opens and the front face of the test sample is exposed by the laser beam. At t=6s (or 11s, or 16s), the reflective shutter is closed and the test sample cools. The temperatures are recorded during 60s.

Test post-processing

The test results for the square plate (test configuration C1) are analyzed with the THIDES method and with the newly ACACIA interfaced methodology in order to compare methods.

The results with THIDES and ACACIA are presented on figure 17. The step signal is well reproduced in both cases. The incoming heat flux amplitude is precisely predicted by the 2 methodologies. A small overshoot can be noted with ACACIA at the establishment of the heating. A negative undershoot is also observed after the heating is stopped. The flux estimation obtained with THIDES does not show the overshoot as the parameter used in the inverse heat conduction methods (time step and number of future time step) can be specially tuned to eliminate the overshoot.

It should be noted that the heating step signal applied for this test is really demanding for the numerical method used to compute the fluxes. As Beck algorithm is a sequential method with future time steps, it is difficult to identify such a discontinuous signal. Nevertheless, the flux identification with ACACIA is totally satisfactory on the steady state. The discrepancies between the 2 methods are linked to non-optimal parameters chosen for ACACIA calculation due to a compromise between calculation time and accuracy. ACACIA method can then be used to analyze more complex configuration.

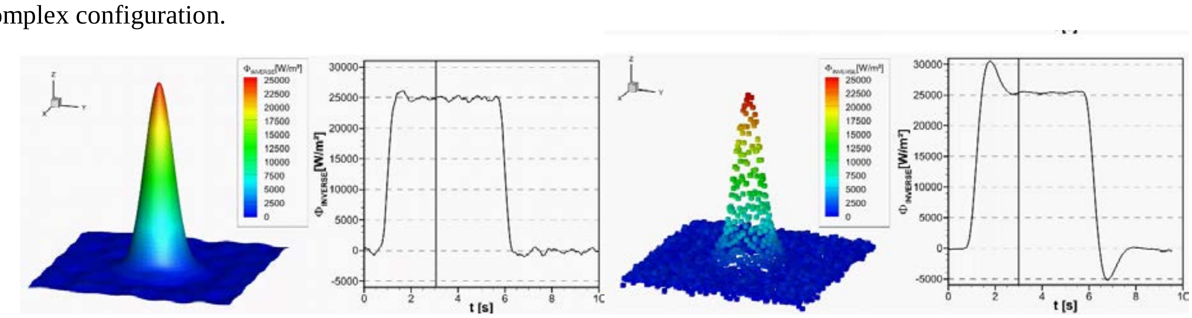

Figure 17: Heat flux restitution with THIDES (left) and ACACIA (right) – Heating time 5s / Heating power 6W

The next step is to apply the ACACIA method to a full cylindrical specimen (configuration C2). This configuration can be analyzed with ACACIA method only as THIDES method is not able to treat such non cartesian geometries.

The heat flux resulting from the cylindrical plain specimen is presented on figure 18 (left). The spatial distribution and time evolution of the heating flux are well predicted. As for the square sample, small overshoots can be noticed at the beginning and ending of the heating phase. The fluxes distribution is not exactly symmetrical. This non-symmetry is caused by the unstructured mesh used to perform the analysis.

The geometry of the cylindrical specimen with 4 holes at injectors' locations (configuration C3) looks more like the CONFORTH configuration. The heat flux obtained for this configuration is presented on figure 18 (right). The flux time evolution and the maximum flux amplitude are well predicted. The fluxes distribution is a little bit uneven around the holes. This spatial distribution is due to a discrepancy between the boundary condition considered in the computation (adiabatic) and the small but not zero heat transfer that occurs at the interface between the cork cap and the disc. Despite this experimental limitation, we can consider that the heat fluxes identification is well executed for such a complex geometry configuration.

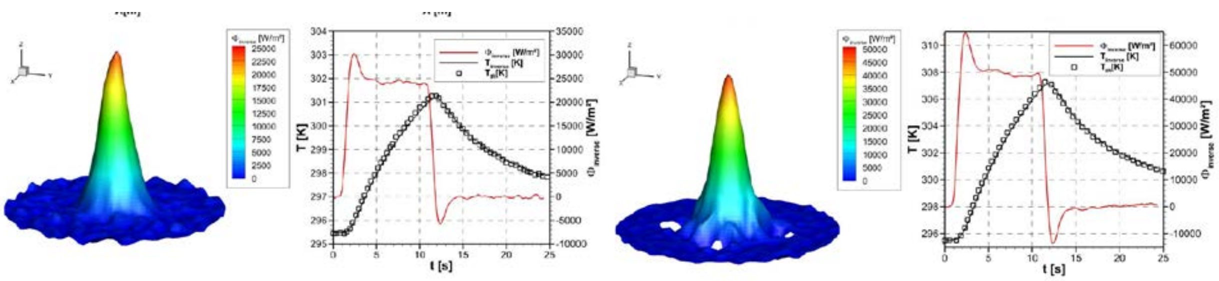

Figure 18: Heat flux restitution with ACACIA - Cylindrical plain specimen (left) / Cylindrical specimen (right) – Heating time 5s / Heating power 12W (left) and 12W (right)

DOI: 10.13009/EUCASS2017-260

The test bench needs to be modified for the latest configuration with the cylindrical specimen including cooling tubes at injectors' locations (C4). As the test sample is equipped with local temperature measurements, the rear optical access used for the IR thermography is not needed anymore. This rear IR window is replaced by an equipped door used for thermocouple connection and coolant pipe feeding.
As said before, the number of local measurement points is limited in comparison with the number of unknown parameter to be determined. It is then necessary to introduce additional assumptions on the heat fluxes distribution.
The unknown heat flux values can be written in the following form:

$$q^n(x,y) = \sum_{i=1}^{N_p} a_i^n . f_i(x,y)$$

Where a_i^n are the parameters to be determined (for the time *n*) and f_i is a function base to be defined, depending of the specific test configuration.
The problem to solve can then be written as a functional to minimize:

$$R = \sum_{i=1}^{N_p} \sum_{j=1}^{r} \left(Y_i^{n+j} - T^{n+j}\left(a_1^{n+1}, a_2^{n+1}, \dots, a_{N_p}^{n+1}\right)\right)^2$$

For the BLADE test facility (and also for CONFORTH), the surface subjected to the heat flux is a disc. So under the assumption that the incoming heat flux is axisymmetric, the function base can be chosen as a set of radial functions.
During the test, the temperature sensors are fitted at 5 radial positions: r= 0,5,10,20 and 30 mm. It is then possible to determine a maximum of 5 independent parameters.
For the BLADE tests, several types of functions have been evaluated: piecewise linear functions, cubic functions, cosine and polynomial functions. The polynomial functions have been used for test post-processing as they give satisfactory results for this configuration (axisymmetric geometry and Gaussian flux).
Each test is repeated several times with different heating times in order to verify repeatability of the test conditions and material thermal response and also in order to evaluate the sensibility to heating duration and heating power.
Figure 19 presents the post-processing results of one test. The time evolution of the heating is correctly reproduced. The maximum amplitude predicted is 15% less than the values predicted in other configurations with IR thermography (C1 to C3). This underestimation can be explained by the little number of parameters to be determined (12 thermocouples but only 5 different equipped diameters) and also by the type of chosen functions. Another important parameter concerns the uncertainty of the sensor location even if during the sample preparation a special care was given to the sensor positioning.
Moreover it should be noted that the external radius of the test specimen is not equipped with any temperature sensor. However the limits of the computational domain are really important for the stabilization of the solution.

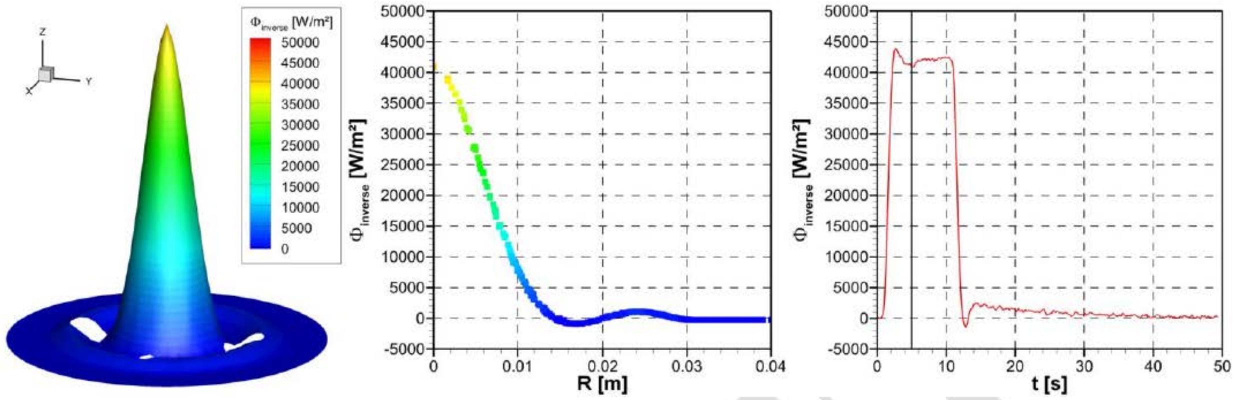

Figure 19: Heat flux restitution – Heating time 5s / Heating power 12W

The post-processing is considered as really satisfactory. This new methodology can now be applied on the CONFORTH injector head.

DOI: 10.13009/EUCASS2017-260

CONFORTH injector head fluxes identification

A gas/gas campaign performed with CONFORTH test set up is chosen to apply the new methodology previously validated.

This campaign took place in 2010. During this gas/gas test, the reactants (H2/O2) are injected at room temperature.

The CONFORTH configuration consists of the instrumented non-cooled injector head, the 2 instrumented water cooled segments and the axisymmetric nozzle.

A typical test sequence is presented on figure 20. The temperature measurements are normalized by a reference temperature, T_R. The normalized temperature, defined as $\theta = T/T_R$ is then plotted versus time.

The test sequence corresponds to high pressure and high mixing ratio operating conditions (P=66 bar, r=7).

The test is initiated by the injection of the cooling flows: helium cooling flows around the injector head and at the entrance of the nozzle convergent and the water cooling of the combustion chamber. Then ignition torch is activated (around *t=24 s*). The torch ignition has a small effect on injector head temperatures. Next, the H2 and O2 flows are started at moderate values *(t=25.5 s*). Temperatures in the injector head suddenly increase during the ignition. At *t=29 s*, the reactant flow rates are increased in order to reach the nominal operating condition. This flow rate increase generates another sharp growth of the temperatures. The operating point is maintained during 6 s in order to reach a thermal steady state. Then at *t=35 s*, the H2/02 valves are closed. The helium flows are kept 15 s longer in order to flush the chamber.

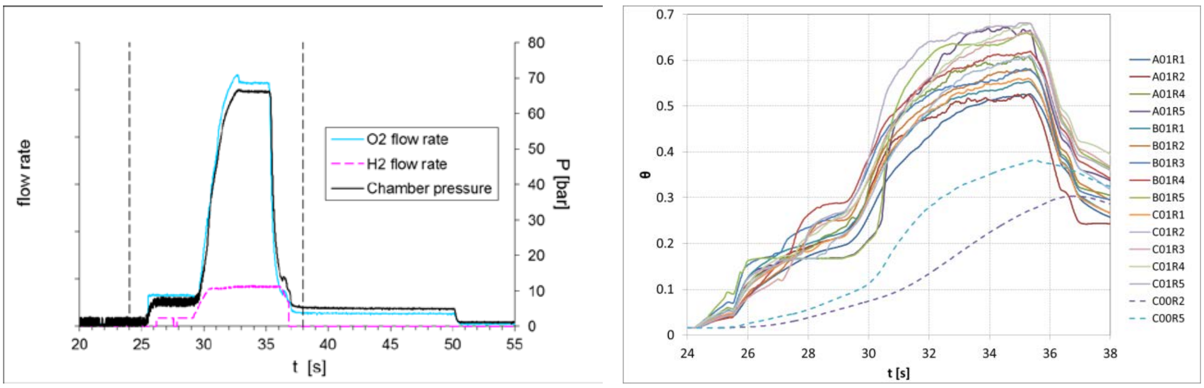

Figure 20: Typical evolution of mass flow rate, pressure (left) and injector head temperatures (right)

The temperatures and operating parameters (pressure, flow rates …) recorded during the steady state of the firing test are used to perform the heat flux identification.

The computation domain used for the flux identification can be reduced to a 45° sector (1/8) thanks to the symmetry of the injector head.

The boundary conditions in the injectors holes is a convective heat flux: temperature is given by the test bench temperature sensors and the heat transfer coefficient is calculated with the Colburn correlation. On the injector face place, the boundary conditions are defined by the convective fluxes to be determined. An adiabatic condition is applied on other faces (rear/lateral).

The flux identification is performed using the methodology validated on the BLADE configuration.

Accounting for the configuration of the injector head and given the little number of temperature sensors during the flux identification, it is assumed that the flux variation can only be radial. Moreover the temperatures are measured at only 4 radial positions so the number of parameters to be determined is limited to 4 parameters.

Several function bases have been used to perform the flux identification: polynomial, cosine and uniform.

On figure 21, the flux radial evolution against the time is presented for the cosine function solution. The fluxes are normalized by a reference flux $\phi_{ref.}$ The normalized flux, defined as $\phi = \varphi/\varphi_{ref}$ is then plotted versus time and radius.

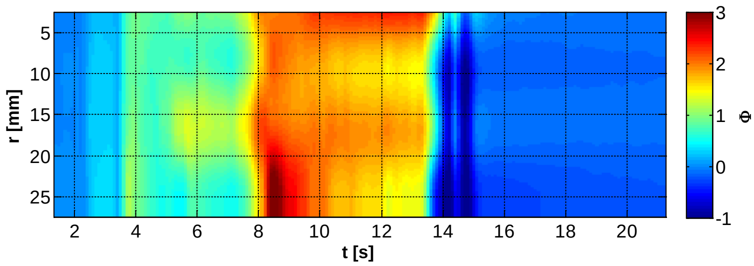

Figure 21: Heat flux time and radial evolution

DOI: 10.13009/EUCASS2017-260

The comparison of the uniform and radial varying fluxes shows that even if the surface average fluxes are very close, some transient differences can be seen during transient phases. During the ignition sequence (t=8.4 s) and (t=13 s), the maximum gap can reach 30% of the uniform flux.
The performance of the flux identification can be represented in terms of the evolution of the function R that is minimized for the resolution of the inverse heat conduction problem. The standard deviation of the differences between the observations and the calculated temperature (function R) is presented on figure 22.

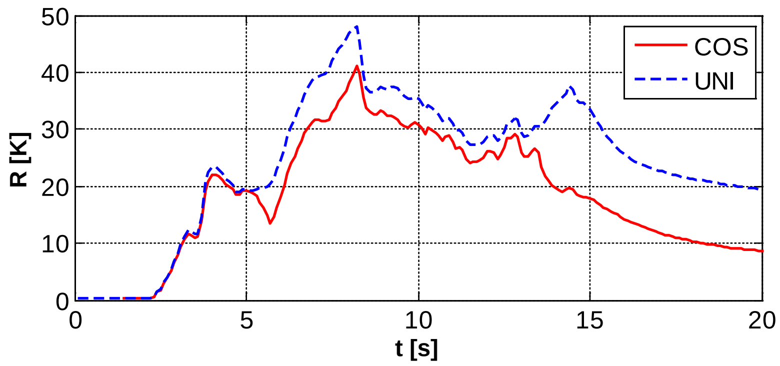

Figure 22: Functional time evolution for cosine and uniform flux distribution

It can be seen that the cosine radial varying solution predicts better temperatures but the difference with the uniform solution is small (5 K) during the firing phase of the test. The temperature difference rises only after shut down.
It was then decided to retain a uniform heat flux distribution model for the injector head flux identification as the uncertainty generated by this choice seems reasonable compared to other uncertainties and assumption of the studied case.
The fluxes obtained for the high pressure, high mixture ratio presented above, are plotted on figure 23. It is possible to identify the different phases of the test sequence:

- Before ignition, the flux is equal to zero as there is no reactant flow in the combustion chamber.
- A first rapid increase, the flux remains at a plateau which corresponds to the low flow rate during the ignition sequence.
- A strong increase of the flux occurs then when the flow rates are set to the nominal operating point. After this peak the flux tends to decrease slowly.
- The sharp drop follows the closing of the reactant valves.

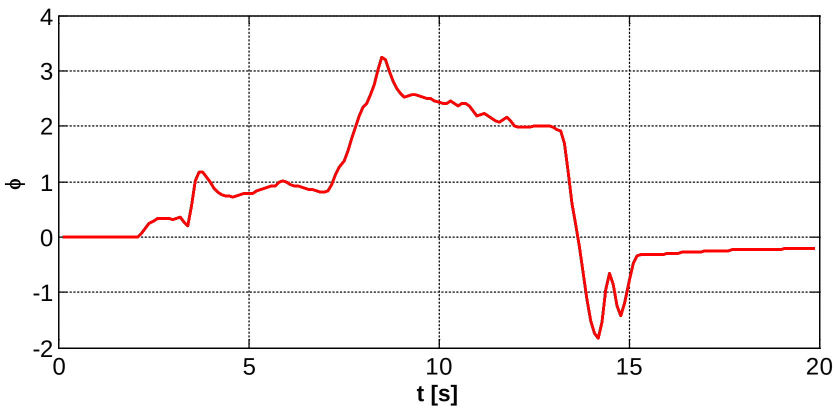

Figure 23: Typical evolution of the identified heat flux on injector face plate

The measured temperatures and the calculated temperatures are presented on figure 24 for the 0° generating line. The calculated temperatures for 3 locations (A01R1, A01R2, A01R4) are very similar since their relative distances to the injector are the same. The calculated temperature for A01R5 position presents a stronger temperature increase as the distance between this point and the injector is larger. The comparison with the measurement shows that the calculated temperatures are globally close to the measurements except for the A01R4 position: the sensor shows a higher temperature increase. This behavior could be explained by the large temperature gradient observed close to the injectors: a small uncertainty on the radial position of a sensor can generate a large difference in the measured

DOI: 10.13009/EUCASS2017-260

temperature. The characterization of this thermal gradient is limited with the current sensors distribution as most of the sensors implemented are at the same sensor-to-injector distance.

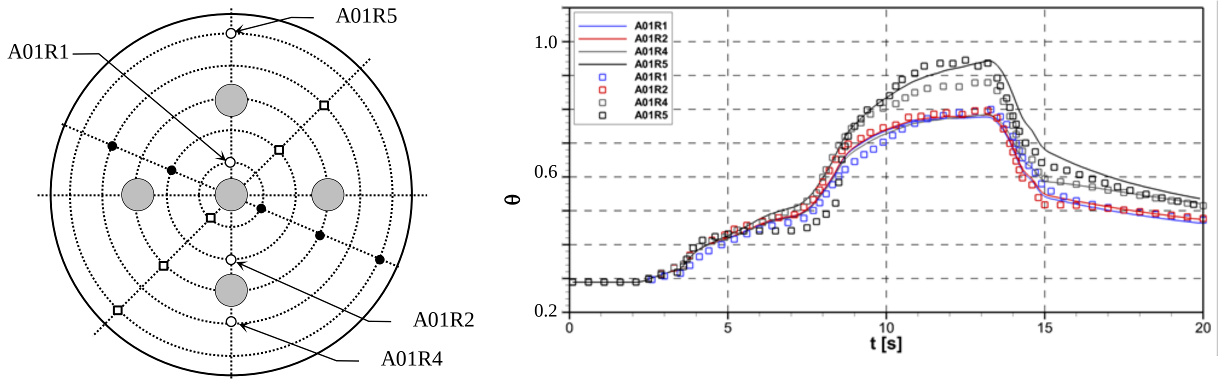

Figure 24: Measured temperatures (symbols) and calculated temperature (plain lines)

Even if a recommendation of a more efficient sensor distribution around the injector can be specified (several sensors implemented at various distances of the injector in the strong gradient area), the results obtained thanks to the new methodology seem satisfactory and promising.

The inverse heat conduction resolution is applied to several tests performed for various operating points and some of the results are presented on figure 25. It appears that for a same operating point (e and f) the heat flux identified are extremely close. The fluxes tend to rise with the pressure increase (for a given mixture ratio). The fluxes decrease if the mixture ratio increases (for a given pressure). The fluxes identified thanks to the new methodology follow then realistic tendencies.

The implementation of this new methodology is considered as really satisfactory as it enables to obtain the relevant heat fluxes for the injector face plate thanks to the temperature sensors embedded in the injector head.

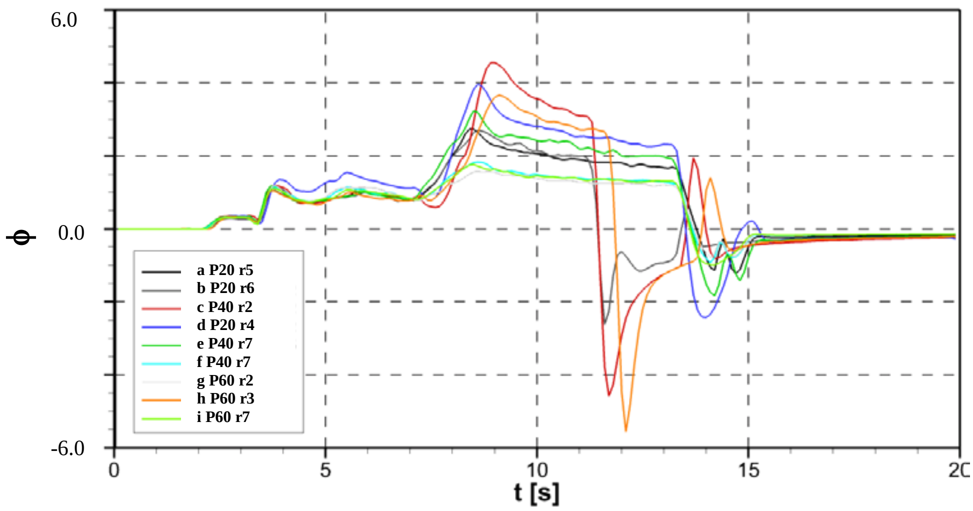

Figure 24: Heat flux on injector face plate for various operating points

Conclusion

Combustion experimental test at subscale is a key element for the knowledge improvement of the design of liquid rocket engines. The CONFORTH test set up has been used to gather an important experimental database of H2/O2 fire tests performed on MASCOTTE bench in a frame of a CNES ONERA common research project.
In an effort to progress in the characterization of the test setup, a dedicated campaign was performed in order to determine the combustion chamber wall temperature distributions for different gas/gas operating points. This campaign permitted to associate an uncertainty range to the data used to perform the validation of the numerical computation methods.
Another major achievement was gained through the improvement of post-processing methods. The identification of the heat fluxes on the injector face plate requires specific methodology as common 1D approach is not applicable. A

DOI: 10.13009/EUCASS2017-260

methodology was then developed and validated by ONERA in order to solve the inverse heat conduction problem for complex 3D geometries with embedded local measurements.
All those efforts in the test setup characterization and post-processing methods development support the confidence in the tools used to build the thermal database. These tools can then be used to investigate more deeply heat transfer within combustion chambers.

References

[1] G.Ordonneau et al. 2011. First results of heat transfer measurements in a new water-cooled combustor on the Mascotte facility, In: *4th European Conference for Aerospace and Space Sciences*
[2] L.H.Dorey et al. 2014 Experimental and Numerical Study of a cooled rocket combustion chamber. In: *15th International Heat Transfert Conference,*
[3] S.Petitot et al. 2014. Heat Transfer and GOX&LOX/GH2 flame imaging in a high-pressure and high-mixture ratio rocket combustor, In: *Space Propulsion-2014*
[4] N.Fdida et al. 2013. Coupling high-speed imaging diagnostics to study a LOX/GH2 flame in a high-pressure rocket combustor, In: *5th European Conference for Aerospace and Space Sciences*
[5] L. Vingert et al. 2015. Improvement of knowledge and modelling of heat transfer in cryogenic combustion chambers. In: *6th European Conference for Aerospace and Space Sciences*
[6] P. Reulet, D. Nortershauser, P. Millan, “Inverse Method Using Infrared Thermography for Surface Temperature and Heat Flux Measurements”, Proceedings of the International Congress on Instrumentation in Aerospace Simulation Facilities, volume 1, pages 118–126, 2003.